Mechanisms of Ground Deformation due to Excavation in Clay

M. D. Bolton *Cambridge University, U. K.*

Abstract

A modern approach to geotechnical construction requires confidence both in the prevention of collapse and the control of deformations. Confidence regarding collapse mechanisms is generally good where soil can properly be treated as a plastic material. Excavations in clay may either lead to plastic flow or to brittle cracking, however. The danger of water-filled cracks in retained earth has long been recognised, but is often poorly understood. The first step to better ground control is to establish the initial stress conditions and the anticipated non-linear behaviour of representative elements. This paper explores the opportunity for using plastic calculations together with raw stress-strain data to obtain a comprehensive understanding of the relationship between deformation, cracking, and collapse. Approximate solutions are valuable in offering a critical framework within which the practising engineer can independently assess the opportunities and dangers of the powerful technique of finite element analysis.

Introduction

The expertise of geotechnical engineers in practice currently rests more in the prediction of collapse mechanisms than ground displacements. Nevertheless, small poorly-controlled trench excavations remain a source of serious accidents on construction sites. Clays especially may appear competent enough not to warrant significant support until cracks open, leading to spalling or toppling failures in trenches, often exacerbated by percolating water. This must be mainly due to poor working practice, because the frequency with which such accidents occur should lead all construction inspectors to forbid any unsupported excavation in ground in circumstances in which workers could be trapped. The trench safety problem may perhaps also be attributed partly to the teaching in soil mechanics given to civil engineers which emphasises the prevention of shear failure, rather than tensile cracking.

Much of the early attention in excavation analysis was devoted to predicting the stresses on the support system: Terzaghi and Peck (1948) applied certain factors to the limiting active

earth pressures to account for the fact that soil strains would not permit full strength mobilisation. Attention to the prediction of these "small" soil strains quickly followed.

Large excavations are increasingly used in congested cities to provide underground space. Here, the removal of soil must be engineered without causing the remaining ground to deform excessively, so that neighbouring structures and services remain undamaged. Where adjacent facilities have to be safeguarded at existing ground level, the lateral support to be provided for the retained soil face must limit vertical and lateral displacements during excavation to an acceptable magnitude. However, what is acceptable depends not only on the magnitude, but also their spatial distribution: this was first addressed systematically by Peck (1969).

The emphasis in excavation technology should therefore be on the control of ground strains, and this must generally be checked in design calculations. Engineers usually rely on demonstrating some factor of safety against collapse: Bjerrum and Eide (1956). The proper definition of factor of safety, and its possible relationship with the magnitude of soil strain, has been a long-standing question. In order to gain further insight, research workers have developed the method of finite element analysis to predict soil strains directly. Some success has been achieved regarding overall behaviour when the non-linear stress-strain behaviour of the ground has been determined, so that appropriate values of soil stiffness could be selected: Burland and Simpson (1974) . However, local behaviour also depends on initial ground conditions, imposed loading, and changing support geometry, which are not necessarily predictable in advance of construction.

Excavation may begin by establishing a full-height in situ wall to support the natural ground, or it may proceed in benches with each step independently supported. Whereas in situ walling was initially restricted to steel sheet-piles, reinforced concrete walls (of the diaphragm or bored-pile type) are now increasingly employed where they can form a useful part of the finished structure. Whereas multiple supports were used to prop faces, it is now also common to specify ground anchors or nails. Evidence regarding the movements induced during the construction of in situ walls has recently been collated and reviewed: Clough and O'Rourke (1990). In all these cases the ground displacements will depend on the composite soil-structure stiffness (which changes as the excavation proceeds), the speed and the sequence of construction in three dimensions, and the degree of skill exercised in fixing the supports. Although the problems of accurately predicting ground displacements are severe, however, the engineer on site does have the advantage of on-line feed-back, with the opportunity to enhance support if problems begin to occur.

The objective of this paper is to show idealised ground deformation mechanisms based on the theory of plasticity and the data of stress path tests. They offer a rational factor against collapse which should also permit the designer to control average ground displacements under working conditions. These mechanisms were suggested after observing physical model behaviour in centrifuge tests, and associated finite element analyses. Their accuracy depends, as all deformation analysis must, on the determination of appropriate stress-strain data, but it is considered a distinct advantage that the non-linear data of stress-path tests can be used directly, with no need to generate artificial soil parameters such as Young's modulus.

Stress paths in soil tests

It is useful, first, to consider the stress paths which will be followed in clay subject to stress relief. Figure 1a shows an effective stress history of two soil elements in the ground; point N′ is normally consolidated with maximum historic stresses, while point C′ has been over-consolidated by factor $\sigma'_{vN'}/\sigma'_{vC'}$ = OCR due to removal of some overburden. For the purposes of clarification, the principal directions will be taken to remain vertical and horizontal through the following sequence of stress changes. The ratio of horizontal to vertical effective stress at N′ is earth pressure coefficient $K_{o,nc} \approx (1 - \sin\phi)$, given by the inverse of gradient ON′. The earth pressure coefficient on rebound at C′ is sometimes given as $K_{o,oc} \approx K_{o,nc}$ OCR^{α}, where Schmidt (1966) suggested $\alpha = 1.2 \sin\phi$.

Figure 1 introduces the maximum shear stress in the plane of shearing $t = (\sigma'_v - \sigma'_h) / 2$, and the mean effective stress $s' = (\sigma'_v + \sigma'_h)/2$, and also shows the result of undisturbed sampling of each element preparatory to triaxial tests. Axes t and s′ are oriented at 45° to the (σ'_v , σ'_h) axes, with a $\sqrt{2}$ scaling factor. The shear stress is lost when the sample is extruded, while the mean effective stress is retained so long as the sample responds in a resilient fashion and is prevented from drawing in water or air: the samples then attain states A′ and B′.

Figure 1b shows in outline the limiting states reachable by samples pre-consolidated to N′. A strong feature are the critical stress ratios K_a and K_p which are the active and passive earth pressure coefficients for clay shearing at constant volume. At small OCRs the clay yields by contracting and then hardens to a critical state. At high OCRs the clay first meets the peak strength envelope of dilatant shear rupture, and then softens to a critical state. The peak strength envelope will show "true cohesion" proportional to σ'_N, but near the origin the tendency to soften to critical states is very strong and the actual mobilisation of unconfined *effective* strength is very doubtful.

Figure 2 shows typical effective stress paths followed in undrained triaxial tests with loading either in vertical compression or horizontal compression (i.e. vertical extension). The vertical compression test from A′ on the normally consolidated sample yields on regaining point N′ and fails at M′. The horizontal compression test from B′ on the over-consolidated sample yields on regaining C′, reaches peak strength at D′ and softens to E′. Overall symmetry about the diagonal s′ axis would be seen only when the clay were isotropic, which is generally not the case. The undrained strengths in compression (active zone) and extension (passive zone) of the normally consolidated sample from A′ would be $t_{M'}$ and $t_{L'}$, while for the overconsolidated sample from B′ they would be $t_{G'}$ and $t_{D'}$. Shear stress t at any intermediate stage can be thought of as the strength "mobilised" at that particular strain, on that stress path.

Points such as G′ and D′ lie on the peak effective strength envelope of shear rupture with dilation suppressed by the formation of excess negative pore pressures, whereas points such as M′ and L′ represent critical state strengths achieved after plastic yielding with contraction suppressed by the formation of excess positive pore pressures. The residual effective stress ratio at points E′ and H′ on the post-rupture path of overconsolidated clay may fall inside the

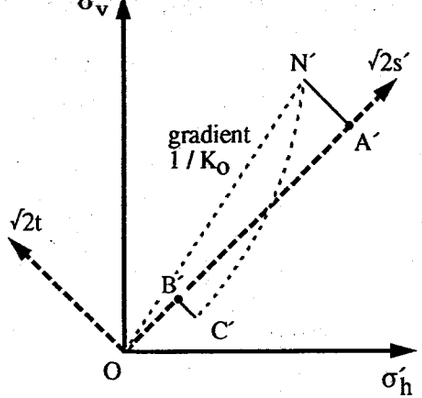

Fig 1a One-dimensional strain paths, followed by sampling

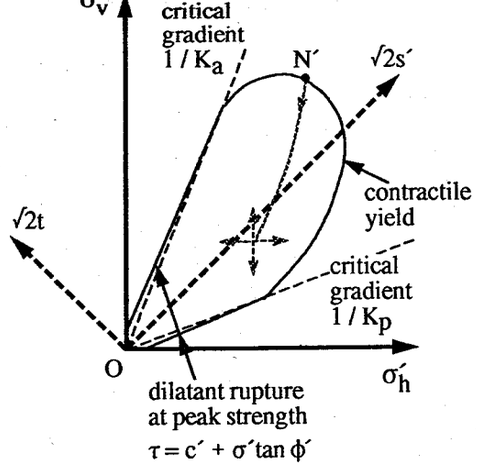

Fig 1b Limiting states for samples over-consolidated from N´

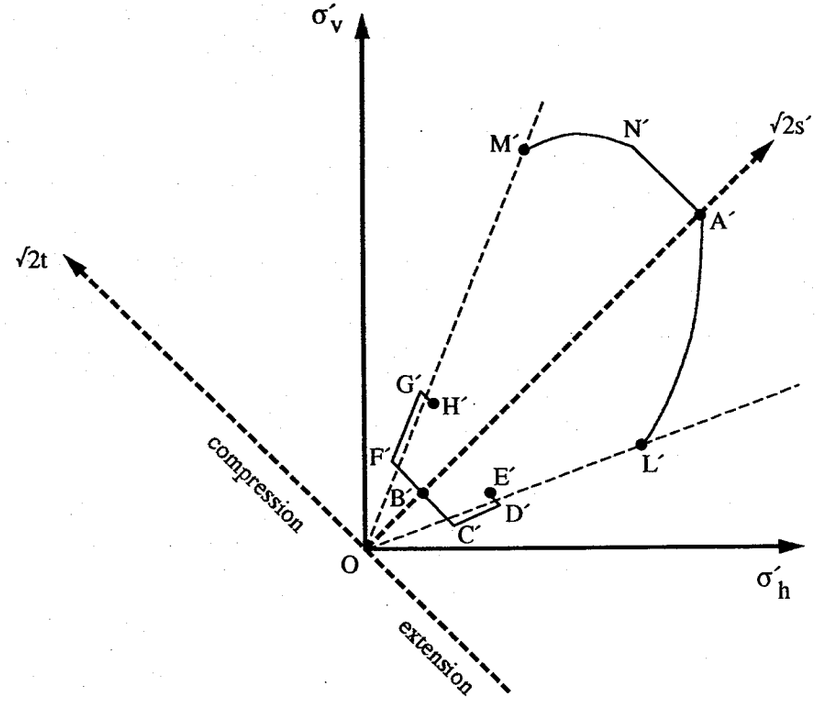

Fig 2 Stylised undrained effective stress paths for oc soil from B´ and nc soil from A´

critical state envelope defined by M´ and L´ at the peak stress ratio of normally consolidated clay, due to the polishing of the softened slip surfaces with continued relative sliding.

Stress paths behind retained faces

The undrained paths to active failure of normally consolidated and overconsolidated clays *in situ* are considered in figure 3, where both total and effective stress paths are shown. In figure 3a the initial pore pressure in situ is taken as zero. The total stress paths remain at constant σ_v consistent with constant overburden while horizontal tensile strain is permitted to induce stress relief: figure 4. The effective stress paths follow the relevant stages of the undrained paths already shown in figure 2. The shading lines drawn parallel to the (√2s, √2s') axis associate total and effective stress points, and represent excess pore pressures on the same √2 scale. Where, as is the case with normally consolidated clay, the total stress at M exceeds the effective stress at M´, the excess pore pressures are positive. Where the reverse is true, as with overconsolidated soil, the excess pore pressures are negative. If the soil in figure 3a can carry tensile horizontal total stress, the excess pore pressure at peak strength would be GG´.

It is unusual for geotechnical engineers to rely on tension, however, and the imposition of a zero-tension criterion (for total stress) limits the mobilisation of active strength to stage XX´. This criterion gives rise to some confusion. Terzaghi's effective stress concept is that the behaviour of the solid skeleton depends only on the effective stresses within it. Evidently, the skeleton at point X´ in figure 3a is far from failure; it is shown in a quasi-elastic state prior to reaching the effective strength envelope at F´. The effective stresses at X´ are safely positive. If the skeleton is now to crack, would this not invalidate the effective stress principle?

The solution to this paradox is found by considering the fluid phase. At some stage WW´ the pore suction ($-u_W$) would fall below either the cavitation limit or the air entry value of the clay. The suction could not increase further, and the total vertical stress must stay constant, so the shear stress t must stay at or below the value t_W which it registered at that point. The response to further horizontal tensile strain must be the tensile failure of the fluid phase, with the sudden propagation of a vertical crack. If atmospheric air enters the crack, the total horizontal stress must drop instantaneously to zero at point X, while the clay close to the crack loses horizontal tension while remaining undrained, so that the effective stress elastically unloads to Y´ in figure 3a.

In the case of a retaining wall, air will probably be trapped on the interface between the wall and the soil during construction, so the water menisci will retreat into the soil as soon as the pore water goes into suction, just after the start of the process at C in figure 3a in which the pore water started at atmospheric pressure. The rupture of the water phase at C, figure 5a, will be followed later by the formation of an open crack at XX´, figure 5b. The pore pressure in the soil will then be negative, and different from the air pressure in the crack. This two-stage process can be reversed later; the crack can close while the wall remains un-wetted, and then the menisci can disappear if the pore pressure in the soil becomes positive once more with respect to the air, so that the air space can flood with pore water.

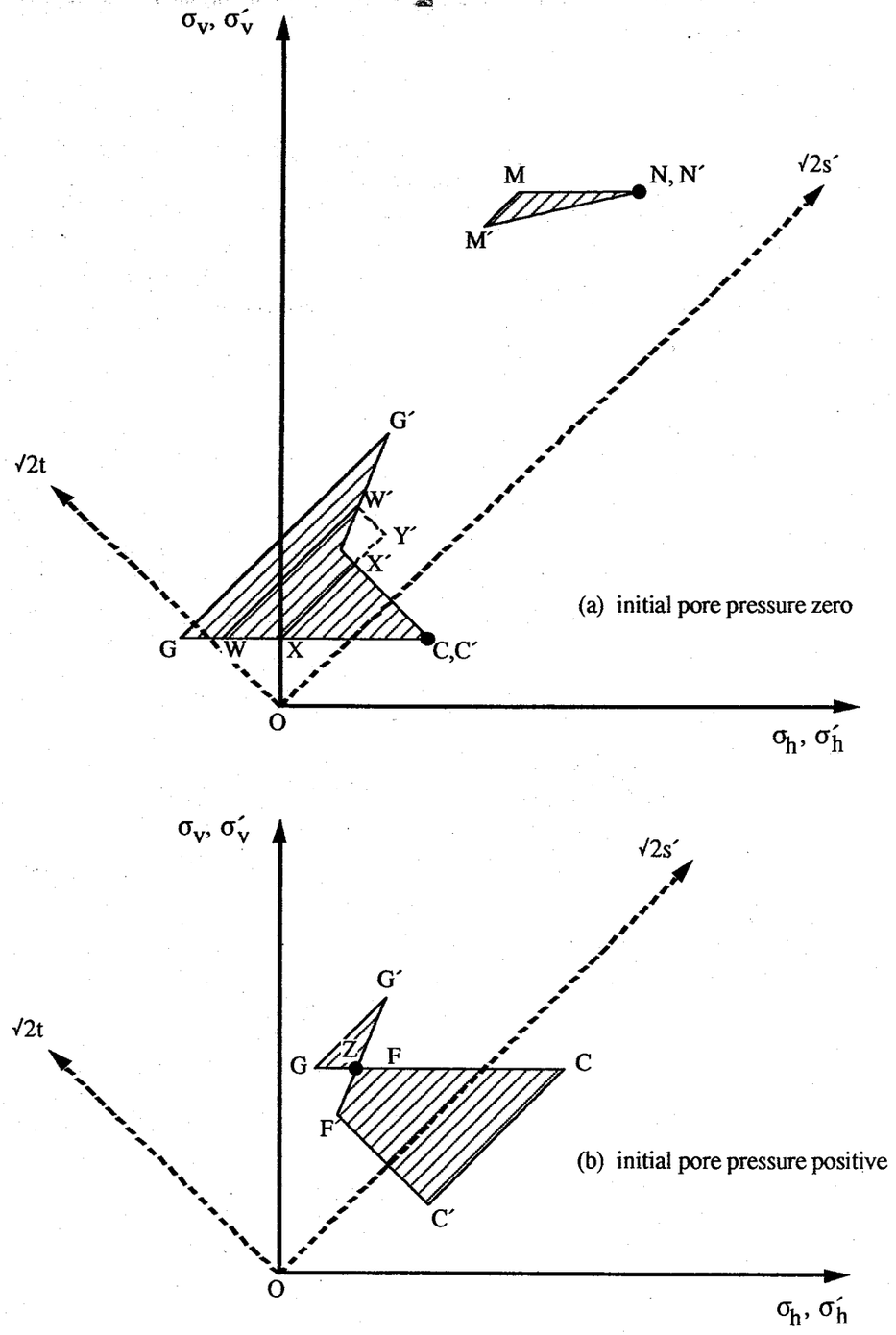

Fig 3 Stress paths in horizontal stress relief

In figure 3b the initial pore pressure is taken to be positive (CC´), corresponding to a point initially below the water table: the whole total stress path is displaced up the $\sqrt{2}$s axis. The absolute values of total stress and pore pressure therefore remain higher throughout by the same amount. The example shown in figure 3b is such that the total horizontal stress can never drop below zero, even at the point of peak strength at G´ at which the undrained shear strength $t_{G'} = c_u$ is being mobilised. However, the pore pressure is shown as negative at G, so the state of clay-wall contact is once again most likely to involve air entry as shown in figure 5a, and the state path will terminate at Z. Although the bulk of the retained clay would be capable of remaining undrained, the contact state at Z satisfies the effective strength envelope and the available wall friction can be written $\tau = \sigma \tan\delta$, where σ is the total stress normal to the wall, and δ is the effective friction angle of soil on wall which can be taken to be ϕ_{crit} for the clay unless the wall material is highly polished. Figures 3 to 5 ignored the effect of wall friction on total stresses, for simplicity.

Eventually, of course, all excess pore pressures will dissipate and the pore pressures will return to their original values unless the long-term groundwater regime has been altered (as it might have been if weep-holes are used to draw down the water table, for example). The final earth pressures will depend on the degree of wall movement permitted during the drained phase. If the wall is held rigid, the effective stress path due to pore pressure rising will be that of 1D swelling, consistent with paths such as N´C´ in figure 1, while if pore pressures must fall the path will veer back towards the 1D compression line ON´. The possible swelling paths following after figure 3 are shown in figure 6 as XJ and ZK. The effective earth pressure coefficients at points such as J´ and K´ are could well be greater than unity if no lateral movement is allowed.

In summary, the response of clay soils to lateral stress relief due to excavation will be:

i) The undrained strength will be mobilized, except where it would involve the generation of suction which could cause de-gassing, cavitation, or air entry. Although the preceding figures tell the whole story, the drawing of total stress and effective stress Mohr circles at peak strength is also useful. Figure 7 shows the possibility of a dry crack extending to depth $z_B = 2c_u/(\rho g)$, with the local negative excess pore pressure at the tip of the crack being $c_u\,(1/\sin\phi - 1)$. If full tensile strength ($\sigma_h = -2c_u$) were to be invoked also at shallow depth A, the negative excess pore pressure would be $c_u\,(1/\sin\phi + 1)$. For a firm clay with undrained strength $c_u = 60$ kPa and effective angle of friction $\phi = 24°$, we would get $u_B = -90$ kPa and $u_A = -210$ kPa. This latter, corresponding to an absolute pore tension of 110 kPa is clearly impossible in normal clay conditions of high saturation, confirming the impossibility of mobilising tensile strength. Neither is the clay body likely to be able to withstand 90 kPa of suction without cavitation or de-gassing. Experimentalists usually find it difficult to maintain 50 kPa of suction even with de-aired samples. Mohr circle B is therefore optimistic: the clay in practice would tend to swell with vapour release. Even quite small negative excess pore pressures are unlikely to be sustained against a wall face: the "wall adhesion" to be expected will usually be wall friction based on the total normal stress (where this exceeds zero).

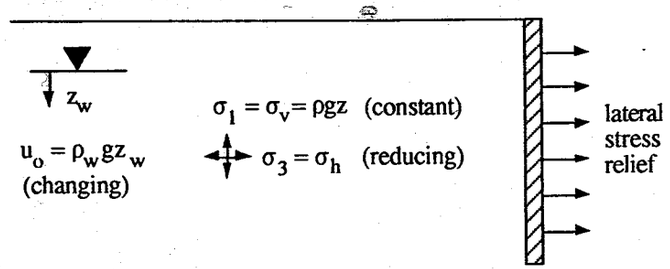

Fig 4 Lateral stress relief (ignoring wall friction)

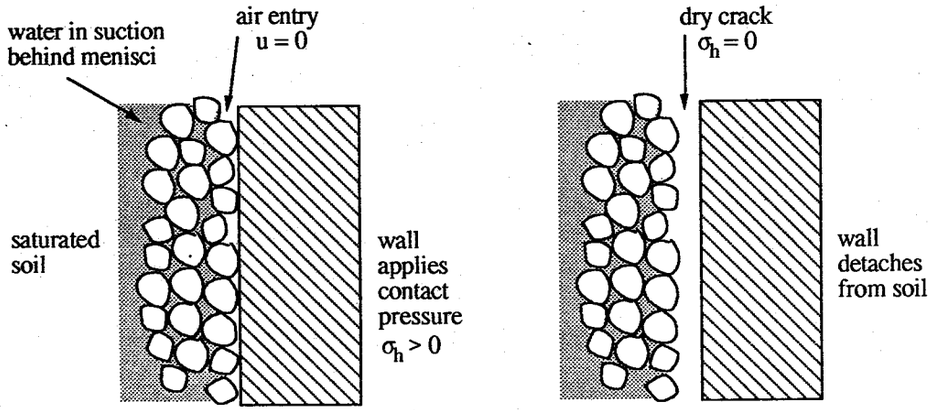

(a) air entry at C in Fig 3 (a)

(b) open crack at X in Fig 3 (a)

Fig 5 Air-entry and cracking against the retained face in clays

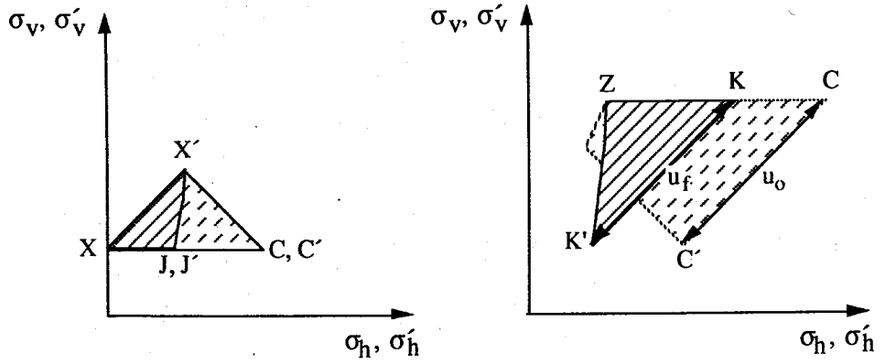

Fig 6 Swelling paths to return initial pore pressures

ii) The pore pressure in the clay and the pressure of gas or fluid in an open crack are quite independent in the short term. Considering the likelihood that vertical tension cracks will occur behind a retained face in clay, and especially on the interface with the wall, it will usually be necessary to consider the possibility that a flash flood, or a burst water main, will be capable of flooding such a crack. Figure 8 shows that the stable depth of a flooded crack extends to $z_C = 2c_u/\{(\rho - \rho_w)g\}$. Above this depth the active wall will be followed out by the water, assuming that sufficient inflow exists to keep the crack topped up. The water in the crack also supports the clay face. At depth z_C the clay itself is able to follow the wall outwards, squeezing hard enough against the face to expel the water and close the crack. The hydraulic thrust adds significantly to the active pressure on the wall, as shown.

iii) In the long term pore pressures will come back into equilibrium, which very likely involves swelling, and may generate large swelling pressures on rigid walls. Flexible or moveable walls may continue to move away from the retained face, of course, and reduce lateral stresses towards their fully drained active values, $K_a \sigma'_v + u$.

Stress paths beneath wide excavations

The response of normally and over-consolidated clays to vertical stress relief following excavation (much wider than the final depth of a clay element) is shown in figure 9. The initial undrained response to a reduction $\Delta\sigma_v$ is an equal reduction $\Delta\sigma_h$ and Δu, leaving the effective stress state unaltered but inducing strong reductions in pore pressure. In figure 9a for over-consolidated clay the total stress point moves from C to Q while the effective stress point Q′ remains at C′. The subsequent drained response involves 1D swelling, such as from C′ to S′ as shown. Since this swelling path for heavily over-consolidated soils also happens initially to run almost parallel to the s′ axis from C′to R′, the total and effective stress paths follow much the same the trajectory, separated by the pore pressure which eventually comes to a small value representing the new water table in the excavation. The heavily over-consolidated clay will end in a state of passive pressure in the shallow region represented by R′S′ in figure 9a. Pore pressures SS′ in the new excavation will be dependent on the long-term ground-water seepage regime.

The normally consolidated soil in figure 9b has a vertical total stress greater than its horizontal total stress, so the undrained removal of the vertical stress tends to induce lateral tension. The initial pore suctions could result in cavitation or air entry, just as with a retained face, and total stress point P in figure 9 could well be unattainable. Any immovable vertical interfaces within the unloaded layer could then be expected to induce tension cracks once the total horizontal stress dropped to zero at point X in figure 9. If an excavation were being carried out inside a rigid caisson, for example, the fast removal of overburden to point X could be accompanied by negligible clay heave while the effective stress state remained at N′, assuming that de-gassing or air entry does not generally occur. At X the clay would begin to peel off the walls of the caisson, so that on completion of the excavation a height of clay equivalent to OX would have detached.

The clay thus affected would behave like an undrained triaxial extension test with vertical stress reducing, and constant (atmospheric) horizontal stress following cracking. During this

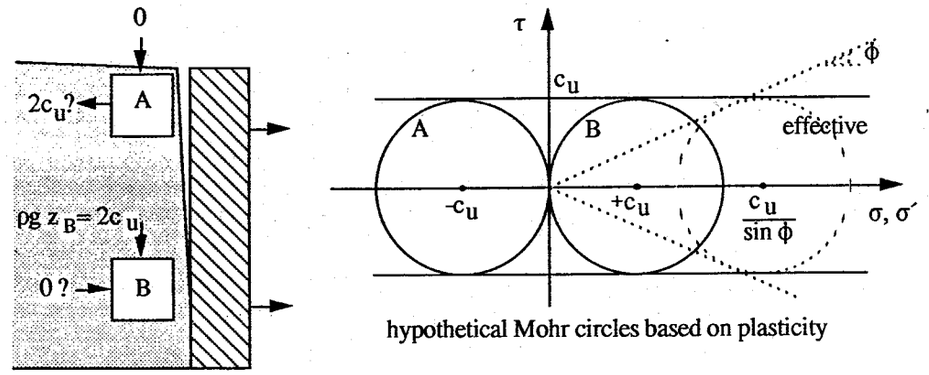

Fig 7 Cracking is not solved by plastic analysis

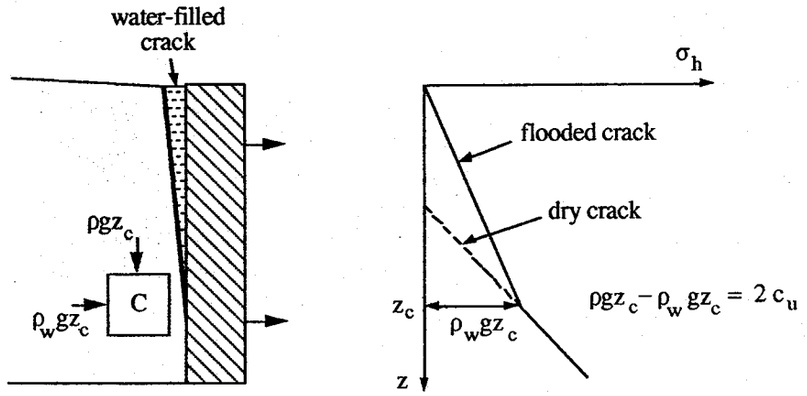

Fig 8 Lateral pressures with a water-filled crack

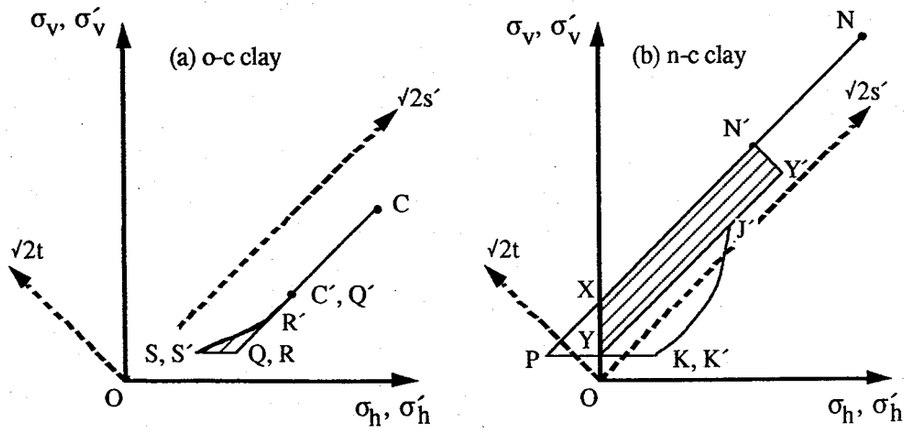

Fig 9 Stress paths in vertical stress relief

later period of undrained unloading the effective stress point would therefore have travelled from N′ to Y′ as the total stress reduced from X to Y. The engineers would observe undrained heave in the excavation, together with vertical cracking, so an appreciable part of the long term heave would already have taken place. Subsequent swelling Y′J′ would first occur in three dimensions until the cracks had healed, so that the subsequent vertical component would be less than it would otherwise have been. Finally, on closure of the cracks at some point J′, one-dimensional swelling would persist until K′ when excess pore suctions had been satisfied. The magnitude of total heave would be difficult to predict, but might not be very much affected by the initial undrained extension phase. A surprising degree of heave during excavation would be the main effect. This would be even more marked if the clay mass were to heave due to de-gassing or air-entry prior to the total stress reaching point X in figure 9b.

Stress-strain testing of clay soils

Undrained tests with pore pressure measurement are essential to establish the envelopes of peak strength expressed in terms of total stress ($t = c_u$) and effective stress ($\tau = c' + \sigma' \tan\phi'$; $t = t_o + s' \sin\phi'$ with $t_o = c' \cos\phi'$) as indicated in figure 2. If it is important to predict soil deformations then the initial state of effective stress in the ground must be estimated. The ground-water regime must, of course, be established. Self-boring pressuremeter tests can be used to estimate in situ horizontal stresses; the subsequent expansion data can be transformed into shear stress-strain plots, with unloading-reloading loops, and pore pressure dissipation tests can also be carried out. Usually, tube samples will be taken. The negative pore pressure registered after high-quality thin-walled tube sampling can be found at the outset of triaxial tests and equated to the mean effective stress in situ, provided no volume change occurred. This offers an alternative method for the estimation of the horizontal stress in situ. On the other hand, if loss of mean effective stress *did* occur – due to cavitation, de-gassing, or air entry –this information will be a useful predictor of similar behaviour in the excavation.

There is bound to be some uncertainty about initial conditions, but it would be good practice to attempt to return the effective stress state of the sample to its in situ value, taking it through an excursion similar to that experienced in the field. In other words, if the in situ state were C′ in figure 1 it would be preferable to sample and then take the element from its state B′ (or a less ideal value with some unwanted swelling or drying) to its preconsolidation state N′, and then return it to C′ prior to conducting any test. A stress path cell with computer control would be required to perform 1D swelling prior to triaxial compression. The swelling path N′C′ is intrinsically valuable, since it permits the measurement of rate of swelling, from which some estimate can be made of the times for pore pressure equilibration in situ. However, the tendency for rates of swelling in the field to exceed laboratory values is exacerbated in unloading problems due to the tendency for de-gassing and cracking already mentioned, in addition to the usual under-estimation of lateral permeability through silt laminae. The results of a 1D swelling test on kaolin are shown in figure 10, with a bi-linear approximation (Bolton and Stewart, 1993) which slightly over-estimates swelling pressures. The shear stress mobilised at high OCR may be written $t = -c_s = r\,\sigma'_{v,max}$ where $r \approx 0.04$ in this case. The "passive" cut-off, evident at $\phi \approx 22°$ in figure 10, was observed when the soil state was

subjected to small load-unload cycles as it swelled, but it seemed to be absent in pure monotonic 1D swelling paths which seemed capable of mobilising $t = -c_s$ up to tensile failure.

A further justification for pre-conditioning the sample with a 1D effective stress cycle is that the immediate past strain path is significant to the immediate future stiffness. The development of proportional undrained shear strength t / c_u with shear strain γ, in figure 11, provides a familiar example of strain history effects.The mobilisation of shear stress with strain along OA might be interrupted by an unloading-reloading loop AB, followed by continued shearing to peak strength at C. When the soil is at state A the stiffness in continuing strain towards C is small, whereas the stiffness in reversing the strain direction towards B is high. It is generally found to be true that reversal of strain direction, whatever mode of strain was being imposed, causes an increase of stiffness. Continuing strain causes the stiffness to deteriorate steadily until the tangent stiffness at peak strength is zero. Similarly, both extension tests and compression tests should be carried out on vertical cores in order to represent the strain paths of both active and passive zones.

In practice, of course, the ideal is rarely achievable. Engineers may well have to take decisions based on the normalised development of undrained shear strength, as in figure 11, together with some re-consolidation and swelling data from oedometer tests. It will be assumed, in what follows, that stress-strain data is available at least for these excursions. For the purposes of demonstration, a power-law has been fitted in figure 11 to the data of over-consolidated kaolin: Bolton and Sun (1991a). The expression

$$\frac{\Delta t}{\Delta t_p} = \left(\frac{\Delta \gamma}{\gamma_p}\right)^b \qquad (1)$$

fits tolerably well for the shear stress-strain changes (Δt, $\Delta\gamma$), especially on a re-loading path from some arbitrary initial shear stress t_i, where γ_p is the shear strain required for the mobilisation of an extra shear stress Δt_p ($= c_u - t_i$) which mobilises the peak shear strength c_u. For $\gamma > \gamma_p$ we must take $\Delta t = \Delta t_p$ so that t remains at c_u. For a new stress path starting after a strain reversal at $t_i = 0$, the values $\Delta t_p = c_u = 70$ kPa at $\gamma_p = 0.06$ with $b = 0.25$ fit the cyclic data of kaolin with an initial OCR in the range 5 to 10. Power curves also fit the data of natural clays: for example, $\Delta t_p = c_u = 160$ kPa at $\gamma_p = 0.03$ with $b = 0.65$ fits the monotonic triaxial data of an "undisturbed" sample of London clay with an initial OCR ≈ 10.

The familiar definitions of shear stress and strain $t = (\sigma_1 - \sigma_3) / 2$ and $\gamma = (\varepsilon_1 - \varepsilon_3)$ are relevant to plane strain problems such as the deformation behind long sheet-pile walls, and plane tests were actually used to provide the data for figure 11. However, triaxial data are more usually available and corresponding definitions will be taken to be $t = (\sigma_a - \sigma_r) / 2$ and $\gamma = (\varepsilon_a - \varepsilon_r) = 1.5\ \varepsilon_a$ in undrained tests. Used in this way, triaxial data overestimate plane deformations in kaolin by a factor of about 1.5, and they may generally be taken to offer conservative bounds to deformation behaviour.

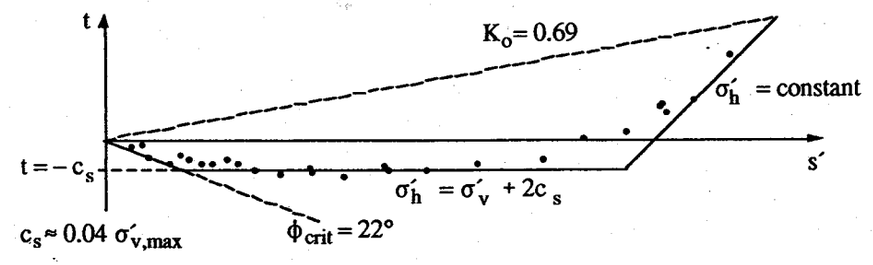

Fig 10 Typical 1D swelling curve for kaolin

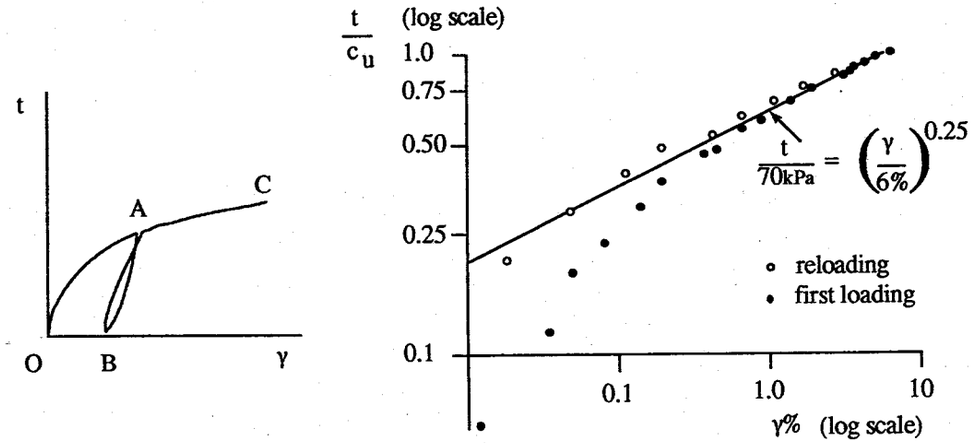

Fig 11 Undrained strength mobilisation in kaolin at OCR ≈ 7

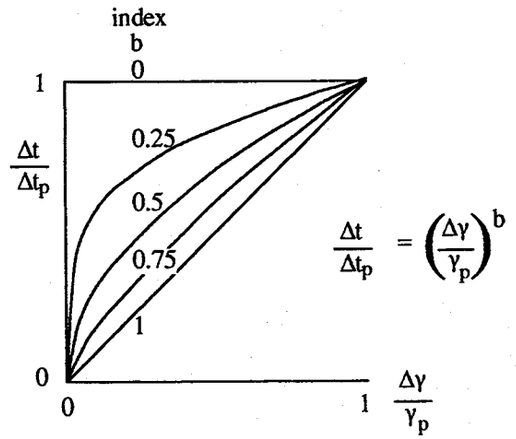

Fig 12 The power index b as a measure of non-linearity

It is appreciated that a variety of empirical relationships could be selected to replace (1), but the power curve has a distinct advantage when the data are to be applied in practice. The exponent b directly expresses the degree of non-linearity. Figure 12 shows that when $b = 1$ the stress-strain curve is linear up to peak strength, when $b = 0$ the material mimics rigid perfectly plastic material, and intermediate non-linearity is given by intermediate values of b. Any curve OAC in figure 11 is to be treated as a plastic hardening relation, similar in nature to the hardening of annealed copper. The soil on loop AB has been hardened to yield stress t_A, and further plastic hardening along the same strain path will carry the strength to its peak value at C.

The "factor of safety" to be applied to the undrained strength of clay depends more on the permissible soil strain than on any uncertainty in the value of strength itself: typical values range from 1.5 in permanent earthworks to 3.0 in foundations. With such large strength reduction factors, the site investigation, testing and analysis would have to be in gross error if collapse were still to occur. But suppose that the engineer could rationally impose a serviceability limit on soil shear strain of 1%, for example. Then pre-cycled kaolin would need a strength reduction factor (c_u / t) of $6.25^{0.25} = 1.6$, while the London clay on first reloading would apparently demand $3^{0.65} = 2.0$. This reduction factor is better called a "mobilisation factor M" rather than a "safety factor F" since it needs to be associated with the permitted degree of soil strain (Bolton, 1993). Evidently, values of M can be chosen rationally with respect to the permissible soil strain, the strain at peak strength, and the degree of non-linearity. From (1), and assuming that some new episode of strain ($\Delta\gamma$) starts at $t_i = 0$, we get:

$$M = \frac{c_u}{t} \qquad (2)$$

$$\Delta\gamma = \frac{\gamma_p}{M^{1/b}} \qquad (3)$$

Geo-structural analysis

The assumption in engineers' beam theory, that only bending moments give rise to deflections, can be viewed from either a theoretical or a practical stand-point. Theoretically, the assumption is an error because it ignores the influence of shear forces. Practically, the assumption can be regarded as a useful simplification and justified on the grounds that the selection of standard steel or concrete sections to meet loading and deflection requirements would almost never be influenced by the shear component. Theoreticians might argue that it is the easy dismissal of shear in beam theory which sometimes leads practising engineers to make errors in the designation of shear reinforcement in concrete beams and slabs. They could point to Timoshenko's complete analysis of stress and strain in beams and ask why graduates are not trained to perform more accurate analyses. Practising engineers might respond that the use of more complex theories in the design of structures could lead to a higher rate of failure due to gross human error.

The argument between theoretical consistency and practical utility will never finally be settled; for example, a finite element program may intervene to provide practising engineers with a complete solution which is also easy to apply. In any event, structural engineers should demand that graduates continue to learn beam theory: how else are they to gain the intuition to take structural decisions? Theoreticians often forget that the objective in design and construction is to take a logical sequence of decisions. It is necessary first to pose the right questions before considering how to get right answers. The civil engineer must first develop an intuition for the various modes of behaviour of steel, concrete, soil and water so that good designs can be proposed. High level analyses are useful only to check the design hypothesis once it has been formulated.

In soil mechanics and foundation engineering, engineers have been in the unhappy position of having no simple but robust theoretical models for ground deformation – no equivalent to engineers' beam theory. If quick estimates of soil displacement were called for, engineers have generally had to rely on elasticity theory. It has long been clear, however, that the stress-strain curves of soil elements are highly non-linear as in figure 11, that they depend on the mode of straining and especially on the degree of drainage permitted, and that plastic failure intervenes in a quite complex way as in figure 2. No rational selection of equivalent-constant elastic stiffness can emerge, and errors of a factor 10 in elastic type calculations are commonplace. Engineers can, of course, ask an expert to run a non-linear finite element program which is claimed to simulate some more complex features, but there is often a difficulty in communication between engineer and analyst concerning the degree of confidence which may be placed on the values to be used for the special parameters which such programs usually invoke.

The objective here is to develop a robust, approximate theory of ground deformations capable of accepting – directly – the raw data of soil tests such as those referred to above. Curve-fitting of stress-strain data will be optional, and strictly for convenience. The technique will be based on plasticity, and will consist of separate treatments of plastic equilibrium and plastic kinematics. Plastic equilibrium calculations are familiar to engineers as the technique they use with peak soil strengths to determine "factor of safety". Here they will be used to find the "mobilised soil strength" required for equilibrium under whatever loading conditions are specified, including safe working loads. This mobilised strength will be used to deduce a mobilised strain from appropriate stress-strain data. The soil strain will then be used to determine ground displacements using an appropriate plastic mechanism. Although the equilibrium mechanism and the kinematic mechanism should ideally be identical, we will have to be satisfied with broad consistency, and tolerant of some errors of detail. This will be more reminiscent of structural analysis than continuum analysis, and the technique will here be called the analysis of "geo-structural mechanisms".

Geo-structural mechanism for lateral stress relief on an undrained clay face

Figure 13 shows the incremental equilibrium solution for a cut face in soil which is unloaded horizontally by a uniform total stress $\Delta\sigma_h$ while the total vertical stress is constant. Principal stresses are taken to remain vertical and horizontal. The Mohr circle of stress

increments shows that an increment in shear stress $\Delta t = \Delta\sigma_h / 2$ is induced on all planes at 45° to the face.

Either by reading directly from a stress path test which starts at the pre-determined in situ stress state, or by assuming the adequacy of an expression such as (1), the increment in shear strain $\Delta\gamma$ is then estimated. Figure 14a shows the typical situation for over-consolidated clay which may be assumed to have commenced a new strain path starting at I with $t_i < 0$, i.e. $\sigma_h > \sigma_v$, and proceeding along the monotonic compression path IM as far as E. Figure 14b demonstrates the difficulty for the predictor who has no knowledge of the origin to be used for strain. Here, the clay has been through a vertical loading–unloading cycle IEJ prior to excavation, so that the initial stresses are unaltered, but the apparent origin for strain J is not the real origin. On excavation, the path returns approximately to E where it resumes its original course to M. Experience of cyclic loading suggests that the increment $\Delta\gamma^*$ in figure 14b will probably be less than one half the increment $\Delta\gamma$ in figure 14a. Uncertainty in strain history or initial stress conditions leads to uncertainty in soil strain predictions and, unfortunately, some such uncertainty will generally be unavoidable.

Figure 15 shows a plastic deformation field consistent with the earlier assumption that principal directions remain vertical and horizontal. The unloaded face is shown rotating outwards by angle $\Delta\theta$, and shearing on planes at 45° produces a similar rotation $\Delta\theta$ in the ground surface behind the wall. Soil beneath the hypotenuse AC remains stationary. The vertical and horizontal strains in the 45° triangle ABC are θ and $-\theta$ respectively (compression positive), and the Mohr circle of strains confirms the geometrical construction that the shear strain increment $\Delta\gamma = 2\Delta\theta$.

Figures 13, 14 and 15 represent the elements of a plastic geo-structural mechanism for lateral stress relief. The engineer can either calculate the face rotation for a given reduction in lateral stress, or can specify a permissible face rotation and ground strain and then deduce the maximum permitted stress relief. If a ground strain of 0.5% is permitted, the face will rotate 0.005 radians, shear strain will be 1%, and the mobilisation factor M will need to be in the region 1.5 to 2.0.

In reviewing the mechanism, it will be seen that the far-field soil displacements outside the near-field active triangle have been set to zero, whereas the lateral stress reduction is assumed to propagate outwards without limit. The solution would be exact if the far-field stiffness were an order of magnitude higher than the near-field stiffness. The very large stiffness of soil at small strains, and the kinematically unfavourable conditions for far-field displacement if the soil face remains stationary at A, should mean that the proposed mechanism is satisfactory for practical purposes. The similarities and differences between the proposed mechanism and the classical Coulomb wedge failure should be noted. Collapse analysis is discussed in terms of absolute shear stresses approaching c_u on the hypotenuse AC while the wedge ABC remains unrealistically rigid. The newly proposed mechanism relates to an increment of shear stress creating an increment of shear strain which is uniform throughout the whole region ABC.

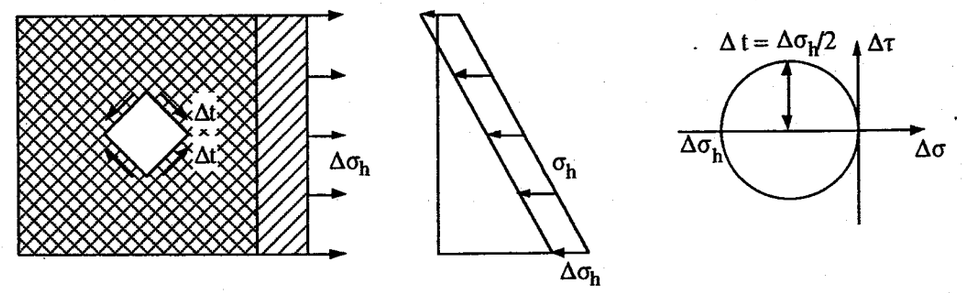

Fig 13 Incremental equilibrium solution for lateral stress relief (assuming zero wall friction)

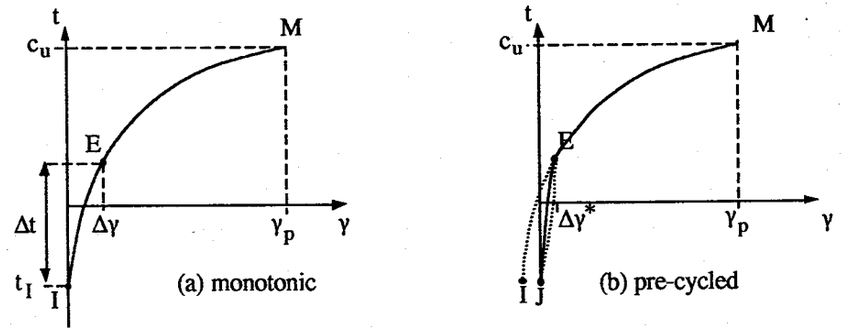

Fig 14 The influence of strain history

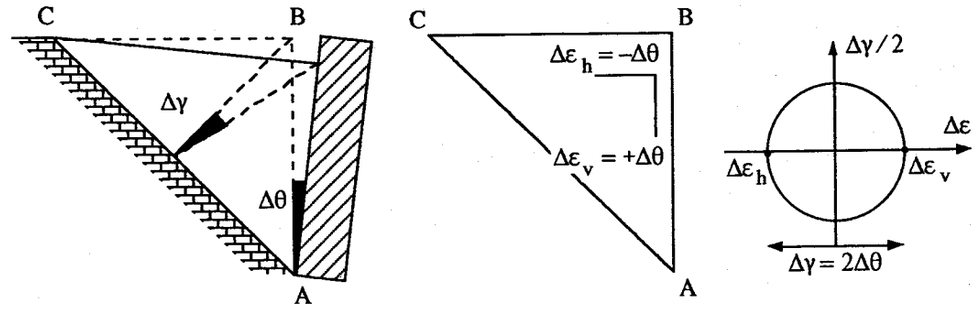

Fig 15 Incremental kinematic solution for wall rotation (assuming zero wall adhesion)

The proposed geo-structural mechanism can accommodate tensile cracking in the same approximate way as current active earth pressure calculations. If the crack is taken as dry and open to a depth h_c against the back face of a wall then, as discussed earlier, the horizontal stress at depth h_c will be zero. Below this point the soil can continue to press against the wall with a lateral pressure reduction of $2\Delta t$ consistent with a soil shear strain $\Delta\gamma = 2\Delta\theta$, where $\Delta\theta$ is the wall rotation as before: see figure 16. It is then clear that the depth of cracking will be such that the pre-existing lateral total stress at that depth equals the calculated amount of lateral stress relief $\Delta\sigma_h = 2\,\Delta t$. Only in the event that the initial earth pressure coefficient was unity would this also equal the pre-existing vertical stress, and only then would the depth of the crack be equal to $2\Delta t / \rho g$.

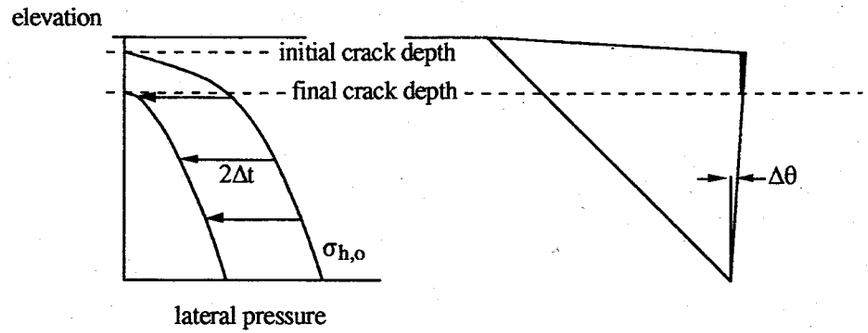

Fig 16 Crack depth as a function of initial lateral pressure and the mobilisation of strength

Mechanism for undrained excavation against a cantilever wall pinned at its toe

The incremental approach to plastic deformation problems using appropriate stress-path data can be extended to provide solutions to some quite difficult problems. For example, Bolton and Sun (1991b) showed good agreement between an incremental hand calculation and the lateral displacement of model bridge abutments with a spread foundations resting on firm clay, observed in centrifuge tests. Figure 17a shows the inevitable kinematics of a stiff in situ wall, socketted into a hard base layer at its toe so that rotation $\Delta\theta$ about its toe is the single degree of freedom permitted to it when an excavation of depth h removes a vertical stress $\Delta\sigma_v = \rho g h$ from the remaining layer of depth d beneath the excavation. Following the compatibility condition sketched in figure 15, the increment of shear strain must be

$$\Delta\gamma_A = \Delta\gamma_P = 2\,\Delta\theta \qquad (4)$$

in both active triangle A and passive triangle P. These shear strains will induce increments of shear stress Δt_A positive and Δt_P negative, so that lateral earth pressure changes $2\Delta t_A$ and $2\Delta t_P$ can be entered as acting to support the wall in the stress increment diagram, figure 17b. The effects of stress relief causing the wall to move towards the excavation are the removal of the pre-existing lateral pressure on the face of the wall exposed by the excavation ($\Delta\sigma_h = \sigma_{h,o}$), and a reduction $\Delta\sigma_h = \Delta\sigma_v$ on the buried face of the wall beneath the excavation, each due to the immediate effect of unloading in the absence of wall movement. Any tendency to cavitation has been ignored here, for simplicity, but a crack of depth h_c should be invoked such that the initial lateral pressure will be just eliminated, $\Delta\sigma_h = 2\Delta t_A$.

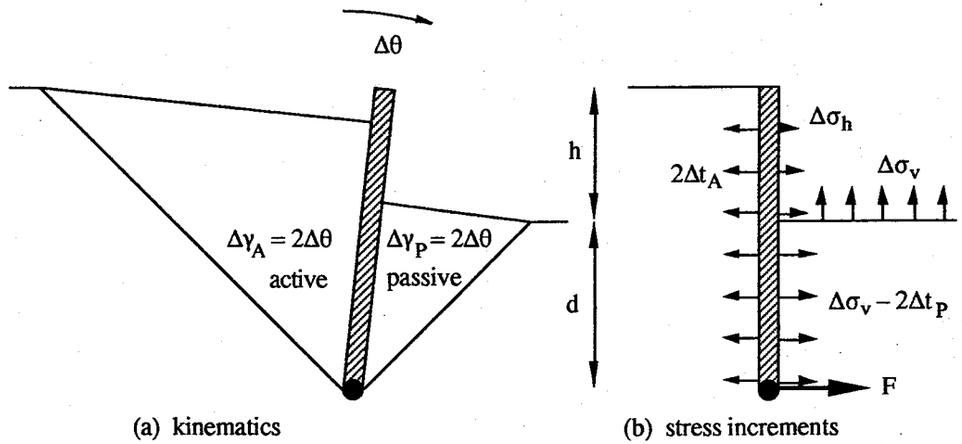

Fig 17 Incremental analysis of a cantilever wall rotating about its toe

Taking moments about the toe of the wall produces an equilibrium equation of the form

$$\Delta t_A\,(h + d - h_c)^2 + \Delta t_P\, d^2 = \Delta\sigma_h \underset{h>h_c}{^{mean}} (h - h_c)\{d + (h - h_c)/3\} + 0.5\,\Delta\sigma_v\, d^2 \qquad (5)$$

where allowance could additionally be made for the moment effect of any other variations with depth in Δt or, especially, non-triangular profiles of $\Delta\sigma_h$. If both Δt_A and Δt_P are known functions of γ, the stepping of $\Delta\gamma$ will reveal a value which solves for equilibrium and compatibility. The method could allow for any amount of anisotropy, and for $K_o \neq 1$, as

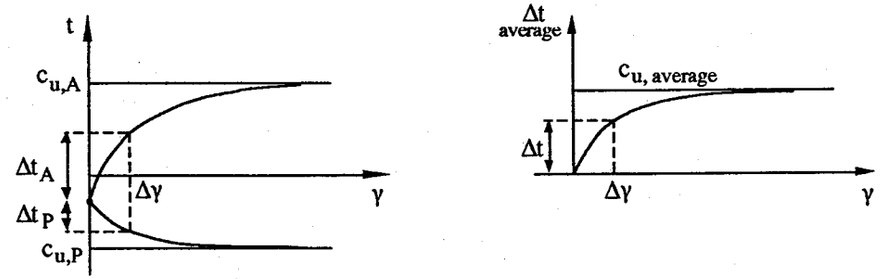

Fig 18 Using stress-strain data

indicated in figure 18a. Characteristic stress-strain data, as in figure 18, is here used directly: there is no need to derive any parameters or even to formalise an equation such as (1). The calculation procedure is ideally suited for a micro-computer running a spread sheet.

While mechanisms such as that in figure 17 permit non-linear analysis based on the typical compression and extension data of figure 18a, engineers will often have only data from triaxial compression tests, or no specific data at all, to guide their decisions. If data on anisotropy does not exist, then some "average" mobilisation curve such as that shown in figure 18b might be derived from triaxial compression tests, but the tendency of extension tests to mobilise less strength should not be forgotten. Likewise, if there is no data on the initial lateral earth pressure, the initial magnitudes of shear stress (e.g. t_I in figure 14) will be unknown and engineers might assume that $t_i \approx 0$. The incremental approach can then be simplified and the final lateral pressures shown in figure 19 can be used in the equilibrium check. Under such circumstances the calculation of displacements can not be expected to perfect, but the geo-structural mechanism can still be shown to offer distinct advantages compared with traditional "factor of safety" approaches.

The only difference between the simplified final pressure diagram in figure 19b and the incremental diagram in 17b is that the mobilised shear strength t_{mob} is assumed to be uniform around the wall, and related to shear strain by the nominal curve in figure 18b. Putting $K_o = 1$ and $\Delta t_A = \Delta t_P = t_{mob}$ in (5) we find the equilibrium condition reduces to

$$\frac{1}{6}\rho g\,(h + d - h_c)^3 = \frac{1}{6}\rho g\, d^3 + \frac{1}{2} 2t_{mob}\, d^2 \qquad (6)$$

where $h_c = 2t_{mob}/\rho g$. At $d/h = 0.5$, $t_{mob}/\rho gh = 0.325$; at $d/h = 2$, $t_{mob}/\rho gh = 0.28$. We must recognise the insensitivity of the mobilised strength to embedment ratio. The more significant parameters in the problem are actually those which we have made nominal for the purposes of figure 19, namely K_o, anisotropy, and variation of strength with depth. For cantilever walls in this range the engineer performing a nominal calculation could safely assume that $t_{mob}/\rho gh = 0.33$ giving $t_{mob}/c_u = 0.33\ \rho gh/c_u$, if an average value c_u can be selected.

Equations (3), (4) and (6) can then be used to give

$$\Delta\theta = \frac{\Delta\gamma}{2} = 0.5\,\frac{\gamma_p}{M^{1/b}} \approx \frac{\gamma_p}{2}\left(\frac{\rho gh}{3c_u}\right)^{1/b} \qquad (7)$$

Although the mobilisation factor M acts numerically in the same way as a safety factor, its relationship to wall rotations is explicit in (7). We showed that to reduce $\Delta\theta$ to below 1/200, factor M in clays might lie in the range 1.5 to 2.0, irrespective of wall penetration. However, the improvement in sensitivity which could follow determination the $\sigma_{h,o}$ and c_u profiles by pressuremeter tests, and anisotropy by appropriate triaxial extension and compression tests, must not be over-looked. The use of finite element solutions which take account of these complexities (Clough and Hansen, 1981; Bolton et al, 1993) should be facilitated if engineers have access to the more direct sort of calculations referred to above.

Geo-structural mechanism for base heave in undrained clay excavations

Terzaghi (1943) viewed base heave in excavations as a bearing capacity problem. Bjerrum and Eide (1956) took the analogy further by using similar shape factors to get a more accurate indication of the stability of 3D excavations, while Eide et al (1972) made a further allowance for wall adhesion. The collapse mechanisms used in these analyses were based on slip surfaces which could not be mobilised at small deformations, and which are therefore not directly relevant to displacements prior to collapse.

Figure 20 shows deformation mechanisms for an excavation which is not propped, so that the sides pinch in as the base heaves. The proposal would be relevant to a face supported by soil nails located within block B. The size of the deforming zone is controlled in (a) by the width e of the excavation, and in (b) by the depth d of the soft material below the base of the excavation. Here, the shape of the foundation bearing mechanism is taken from the statical solution of Prandtl (1920), but the kinematics of the proposed deformation field beneath the level of the excavation is developed from Bykovtsev (1961). If block B offered no resistance to the lateral spreading of active triangle A, and was free to crack away at C from the ground remote from the excavation, the equilibrium analysis of this deformation mechanism would offer the same solution as Prandtl's to the problem of punch indentation in rigid-plastic material - which is regarded as formally correct. An infinitely large number of deformation mechanisms can be found which are kinematically admissible, and which offer identical collapse loads.

What is most relevant here, however, is that the particular deformations shown in figure 20 do not invoke any discontinuous displacements: there are no slip lines, but only diffuse shear strains. These mechanisms can therefore be applied during the strain-hardening phase of soil behaviour prior to peak strength. It is well-known in metal-forming that diffuse shear deformation mechanisms are those observed when strain-hardening is significant: Szczepinski (1979). Bolton and Sun (1991a) calculated the shear strains in relation to boundary displacements for a simple footing. If the block B in case (a) rotates by angle $\Delta\theta$ towards the excavation, it can be shown that the shear strain increments are: $2\Delta\theta$ in active triangle A, $4\Delta\theta$ in passive triangle P, and variable with a mean value of $4\Delta\theta$ in fan F. A similar result holds in case (b) except that the one-sided mechanism produces only $2\Delta\theta$ of shear strain in triangle P. The mean shear strain increments within the area of the plastic foundation mechanisms can then easily by calculated to be

$$\Delta\gamma \approx 3.3\Delta\theta \quad \text{in case (a)}$$
$$\Delta\gamma \approx 2.9\Delta\theta \quad \text{in case (b)} \qquad (8)$$

It is also easy to see that the maximum vertical heave due to the activation of the near-field plastic mechanism on undrained excavation would be:

$$\Delta v_n = e\Delta\theta \quad \text{in case (a)}$$
$$\Delta v_n = \sqrt{2}\, d\Delta\theta \quad \text{in case (b)} \qquad (9)$$

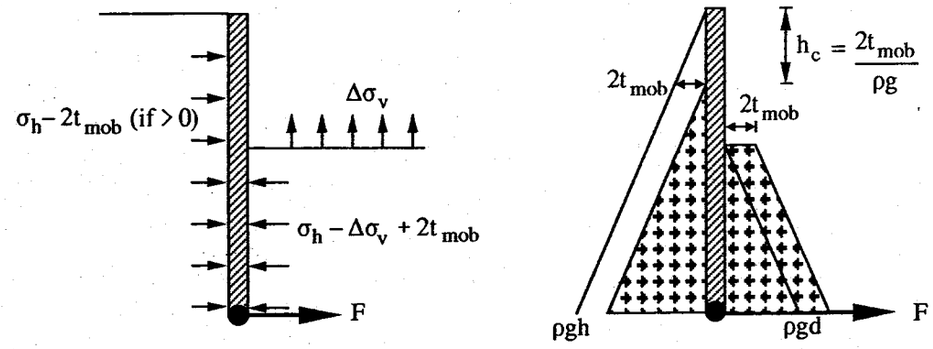

(a) final stresses (b) stresses for beam analysis

Fig 19 Conventional analysis of equilibrium after excavation with K_o=1

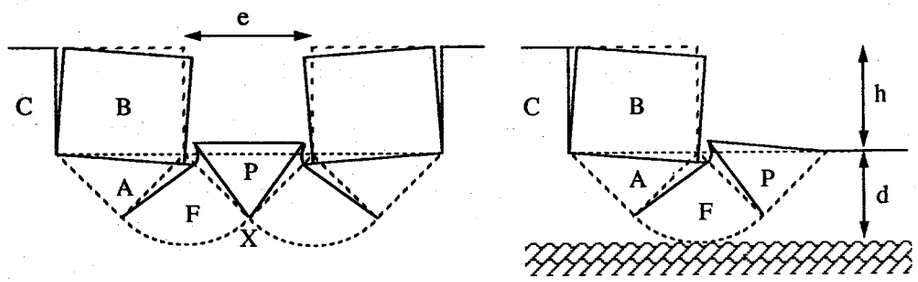

(a) width-restricted mechanism (b) depth-restricted mechanism

Fig 20 Base heave deformation mechanisms for unsupported excavations

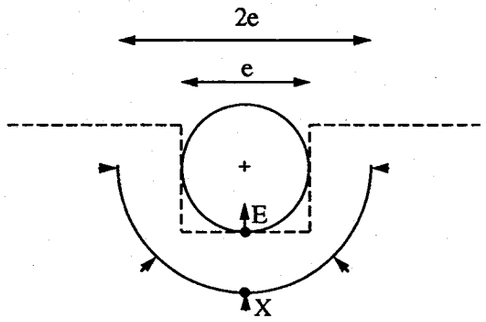

Fig 21 Cylindrical cavity collapse analogy

In case (a) there must be some additional heave due to soil strains in the far field, below the apex X of triangle P. The mobilised strength drops rapidly beneath the Prandtl zone, however, so soil non-linearity has the effect of curtailing strains very rapidly. Preliminary investigation using finite element analysis shows that even in the worst cases in which soil strength does not increase with depth, and the depth of the clay is very large, the extra far-field contribution to undrained heave does not appear to exceed that of the near-field. This approximation can also be appreciated using a cavity collapse analogy. Figure 21 shows the excavation idealised as a cylinder of diameter e which contracts by an amount Δv_E at its boundary E, and the far-field zone lying beyond point X as an infinite cylinder with inside diameter 2e. Continuity of volume in a cylindrical deformation mode demands that

$$\Delta v_E.\pi.e = \Delta v_X.\pi.2e$$

so

$$\Delta v_E = 2\,\Delta v_X \qquad (10)$$

Here, the heave due to strains in the far field beyond X is simply $\Delta v_f = \Delta v_X$, and the total heave $\Delta v = \Delta v_E$, so the heave due to near-field strains must be $\Delta v_n = \Delta v_E - \Delta v_X$. Substituting (9) we obtain

$$\Delta v = \Delta v_n + \Delta v_f = 2\Delta v_n \qquad (11)$$

The cylindrical analogy therefore suggests that the heave due to near-field strains should be doubled in order to estimate the total undrained heave of a deep bed of soil. Applying this rule to (9) case (a), and substituting from (8) for $\Delta\theta$ in terms of the mean shear strain $\Delta\gamma$ in the near-field, we obtain

$$\Delta\gamma \approx 1.7\frac{\Delta v}{e} \quad \text{in case (a)}$$

$$\Delta\gamma \approx 2.0\frac{\Delta v}{d} \quad \text{in case (b)} \qquad (12)$$

Engineers in practice are free to analyse their works in whatever degree of precision is called for, but some simple serviceability criterion would be desirable during design and decision-making. Taking all aspects of the kinematics into account, a useful rule of thumb appears to be:

$$\Delta\gamma \approx 2\,\Delta\omega \qquad (13)$$

where the proportional heave is taken to be the maximum undrained vertical displacement in the excavation divided by the controlling constriction of the mechanism, i.e. $\Delta\omega = v / e$ in case (a), and v / d in case (b).

The plastic equilibrium equation, which engineers have previously employed only at collapse, can be written

$$t_{mob} = \frac{\rho g h}{N_c} \qquad (14)$$

where t_{mob} is the mean strength mobilised within the near-field plastic mechanism. Here, Prandtl's $N_c = (\pi + 2)$ would generally offer a safe lower bound neglecting, as indicated above, the strength of soil on the interface BC. Careful consideration must be given to the possibility of cracking on that interface, however. For example, if water could enter a crack at C and be retained, the vertical component of the thrust from block B on to block A would remain constant, but the resultant would be inclined to the vertical at angle

$$\delta = \tan^{-1}\left(\frac{h\rho_w}{2b\rho}\right) \qquad (15)$$

This would have a large effect on N_c, and would also somewhat alter the deformation mechanism. The case of a rigid block under inclined loads causing deformation of a clay layer was considered by Bolton and Sun (1991b).

Taking an appropriate value of N_c from the best available analysis of plastic equilibrium, the kinematics of (13) can be connected with the equilibrium of (14) using the mean data of stress-strain curves as shown in figure 18, or by the fitting of a power curve such as (1) in the fashion of figure 11 which then offers the estimate of the proportional heave:

$$\Delta\omega = \frac{\gamma_p}{2}\left(\frac{\rho g h}{N_c c_u}\right)^{1/b} \qquad (16)$$

where the inverse of term in brackets would previously have been referred to as the safety factor F and now is referred to as the mobilisation factor M. In this regard, the similarity between (16) and (7) can be taken as a general property of these problems of mobilising plastic strength along a mean power curve.

Figure 22 shows analogous mechanisms for excavations which are sufficiently well-propped to force the retained soil in block B to sink vertically behind the face. Block B behaves somewhat like material emptying from a rough hopper, where the outer interface C is the hopper wall, and the inner sheeted face might either act as the other wall of the hopper (if significant friction can be developed against sheeting which is prevented from sinking with the soil) or as the hopper centre-line (if vertical friction at the sheets should be discounted). In what follows, friction against the sheet is ignored, and the subsidence of the surface of block B is assumed to increase linearly up to the face. Other assumptions are possible.

Neither the kinematics nor the equilibrium equations appropriate to strongly supported excavations are currently as well-understood as in the case of unsupported excavations, partly due to uncertainty regarding cracking which was discussed earlier. The tendency of the top left corner of block B to crack away from C could be suppressed if the propping system at S were sufficiently pre-compressed. On the other hand, we have shown that the attempt to mobilise undrained strength at zero total stress leads to unbelievable pore suctions, and the likelihood of de-gassing into opening fissures. Figure 23 shows a detail of the region BC which is consistent with tensile cracking taking place at 45° within a block which subsides vertically. The cracked zone succeeds in resting its full weight on the top of the mechanism, but shear strength is lost over a height $h_c = t_{mob}/\rho g$.

The best approach to equilibrium which can currently be achieved here is to perform a virtual work calculation assuming that the deformations are as indicated in figure 22. Suppose that the ground rotation is $\Delta\theta$ as shown, mobilising an average soil shear strength t_{mob}. Now consider an infinitesimal additional displacement $\delta\theta$. The additional loss of potential energy is given by the weight of soil in the triangular depression effectively falling a height h to form the equivalent triangular zone of heave:

$$\delta(P.E.) = 0.5\rho g r^2 \delta\theta h \qquad (17)$$

The additional plastic work is due to shear strains $\delta\gamma = \delta\theta$ in blocks B, Q, P and $\delta\gamma = 2\delta\theta$ in the circular fans F. These work against the shear strength to give dissipation $t_{mob}\delta\gamma$ per unit area. The additional plastic dissipation for case (a) in figure 22 is therefore:

$$\delta(P.D.) = (h + 2d - h_c)\, r\, \delta\theta\, t_{mob} + \frac{\pi r^2}{2}\, 2\delta\theta\, t_{mob} \qquad (18)$$

Equating (17) and (18) and re-organising, we obtain

$$t_{mob} = \frac{\rho g h}{N_c} = \frac{\rho g h}{2\left[\pi + \frac{(h + 2d - h_c)}{r}\right]} \qquad (19)$$

Likewise the mean mobilised shear strain can be obtained from an average over the whole area of the mechanism

$$\Delta\gamma = \Delta\theta\, \frac{[(h + 2d - h_c)r + \pi r^2]}{[(h + 2d - h_c)r + 0.5\pi r^2]} \approx 1.5\, \Delta\theta \qquad (20)$$

The mean relation between t_{mob} and $\Delta\gamma$ can be used as before to permit an estimation of $\Delta\theta$ for a given geometry of excavation. It must be recalled that assumptions have been made about the shape of the deformed soil mass, the cracking of the retained soil, the sheets generating negligible friction, and the supports remaining undeformed. The calculation has

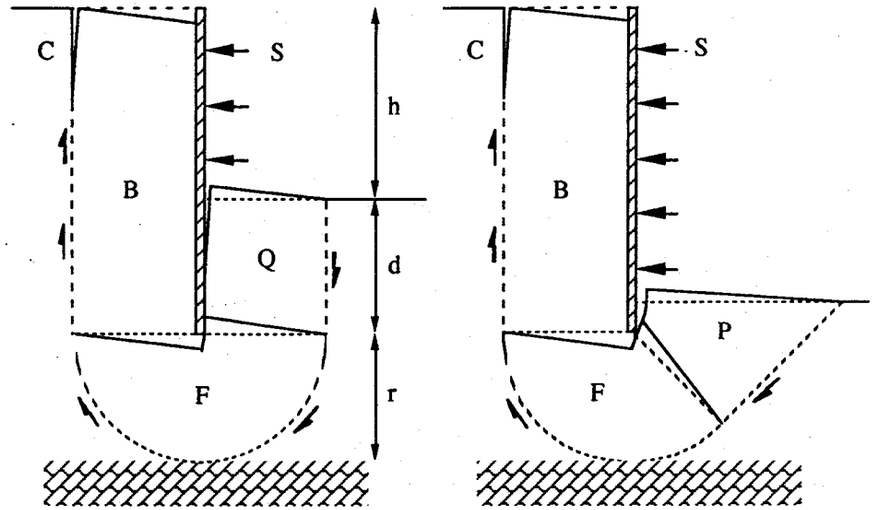

(a) deep cut-off (b) shallow cut-off

Fig 22 Base heave deformation mechanisms for strongly supported excavations

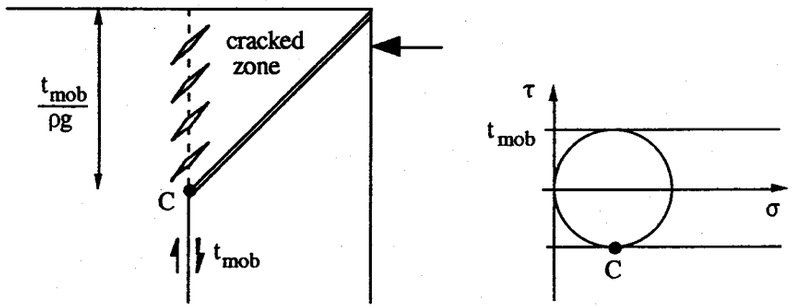

Fig 23 Possible zone of cracking behind a propped face

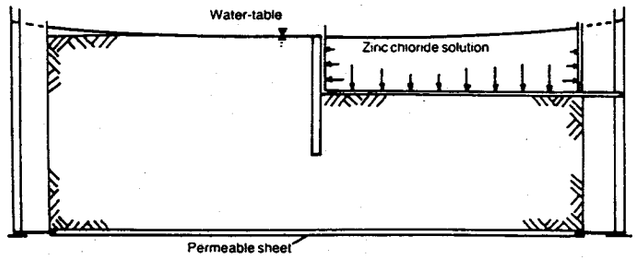

Figure 24 Arrangement of Cambridge tests on model diaphragm walls

rather the spirit of a "limit equilibrium" calculation, whilst being targetted at working displacements.

Figure 21 concerned the problem of a relatively stiff sheet structure which was not fixed at bed-rock, and which therefore permitted base heave and external subsidence as clay flowed beneath it. O'Rourke (1992) considered the case of a flexible sheet penetrating the deforming clay, adding the strain energy of the sheet in to the work equation. He demonstrated that the consequential small reduction in soil strength required for equilibrium could lead to a significant reduction in soil and wall displacements, drawing on the non-linear stress-strain response of the soil.

The ground deformation mechanisms shown figures 17, 20 and 22 are based mainly on theory. Their advantage is that they predict much the same collapse loads as current methods based on slip surfaces, but they invoke distributed shear strains which permit an estimation of displacements under working loads. At the least, they permit a rational choice of the necessary strength reduction factor, taking strains to failure and soil non-linearity into account. They must be used with caution in predicting displacement distributions until further evidence is available to confirm or refine them. They are not a substitute for careful numerical analysis, where that can be justified.

They do, however, suggest an alternative presentation for charts of ground movement around excavations – most of which are expressed as (settlement / excavation depth) plotted against (distance from excavation / depth of excavation), following Peck (1969). It has now been shown that the kinematics of soil movements are dictated by some controlling dimension which will be different in different cases. For excavations with walls permitted significant lateral displacement but avoiding deep-seated base heave, as in figure 17, the dimension will be the height over which wall movement is permitted. This will be the depth of excavation in the case of a flexible face supported by struts, but would be the depth of the wall in the case of a stiff reinforced concrete wall penetrating below formation level. For walls on deep clays which do not gain much in strength or stiffness at depth, deep-seated base heave will control the spread of movements, as in figures 20 and 22. Movements should then be related to the smaller of the width of the excavation, and the depth of soft clay beneath the cut-off. It would be valuable in future if an appropriate controlling dimension were used to normalise both ground displacements and proportional separations.

Tests on model retaining walls

Bolton and Powrie (1987, 1988) reported centrifuge tests conducted at Cambridge, intended to simulate excavation against a diaphragm wall in stiff clay. Figure 24 shows the general scheme in which a block of kaolin pre-consolidated to 1250 kPa was cut to receive a stiff wall supported by a rubber bag containing a heavy fluid. The fluid, zinc chloride, was used to replace the weight of the clay in the excavation, and the model site was brought into equilibrium with a groundwater level at ground level, prior to draining the fluid away simulating excavation. Although convenient, the heavy fluid technique is capable only of pre-conditioning ground with an earth pressure coefficient of unity. Tests in soft clay recently reported by Kimura et al (1993) featured an excavator blade, so that the soil could

independently be given the required stress history prior to excavation in flight in the centrifuge at the Tokyo Institute of Technology.

The Cambridge tests were conducted in a plane strain container at 1/125 scale and all pertained to the removal of h = 10 m (prototype) of clay. Some results will be shown at prototype scale. The profile of undrained shear strength measurable in triaxial compression just prior to excavation was estimated from the testing of samples; it increased from about 50 kPa at 2m depth to 100 kPa at 20m. Real soil profiles in stiff clay show a similar increase of strength with depth. The depth of of the walls varied from 15 m to 30 m, and the full depth of the clay remained at 32 m.

Figure 25 shows soil displacement vectors observed immediately after "excavation" by photography of the cross-section, through a thick window. Freely embedded walls of 5 m and 10 m penetration failed rapidly on excavation due to the tendency of a small amount of surface water to flow into the depression caused at excavation, followed by the opening and flooding of a crack against the wall. The passive resistance of the clay was insufficient to hold a full-height flooded crack as the wall rotated about a point above the toe. Free walls of deeper penetration also rotated about a point near their toe, the magnitude of that rotation reducing by roughly a factor of 2 as the penetration increased from 15 m to 20 m. All these free walls were analysed using the geo-structural mechanism idealised in figure 26. Evidently, there was no need to account for deep base heave in these stiff clays, even when there was sufficient room for a mechanism such as figure 20b to develop. This may be attributed to the relatively large strength which needed to be mobilised to stop the walls rotating, compared with that which needed to be mobilised in preventing deep-seated heave. It arises directly from the calculations of the different mechanisms. Kimura et al (1993) remark on the similar tendency for strength increasing with depth in soft clay to suppress displacements at depth and lead to the rotation of free walls about the toe.

The mechanism in figure 26 is very similar to that in figure 19, except that now there are two degrees of freedom, the rotation θ and the height y of the point of rotation above the toe. These can be found from the two equations of horizontal and rotational equilibrium. An analysis in which tension cracks filled with water correctly predicted the immediate failure of the two shallow penetration walls. For walls of deeper penetration, the pressure distributions based on mobilised active and passive strengths were shown to be in reasonable agreement with measured bending moments. The predicted displacements based on the mechanism of figure 26 and the data of strength mobilised in undrained triaxial and plane compression tests were also encouragingly close to the observations. Best agreement was found by invoking full wall friction ($\delta_{mob} = \phi_{mob}$) in an effective stress analysis using observed pore pressures. In such cases it has proved acceptable to alter the equilibrium equation to account for the wall friction, but to retain the kinematic equation linking soil shear strain to wall rotation.

All free cantilevers rotated excessively if the initial water table was high, so propped retaining walls were included in the same programme. Figure 27 shows two versions of the kinematics of stiff walls rotating about a prop at their crest. In case (a) the soil is forced to deform only within two square boxes, one active and one passive, each split diagonally from the toe of the wall. These boxes are separated artificially from the far field by perfectly smooth

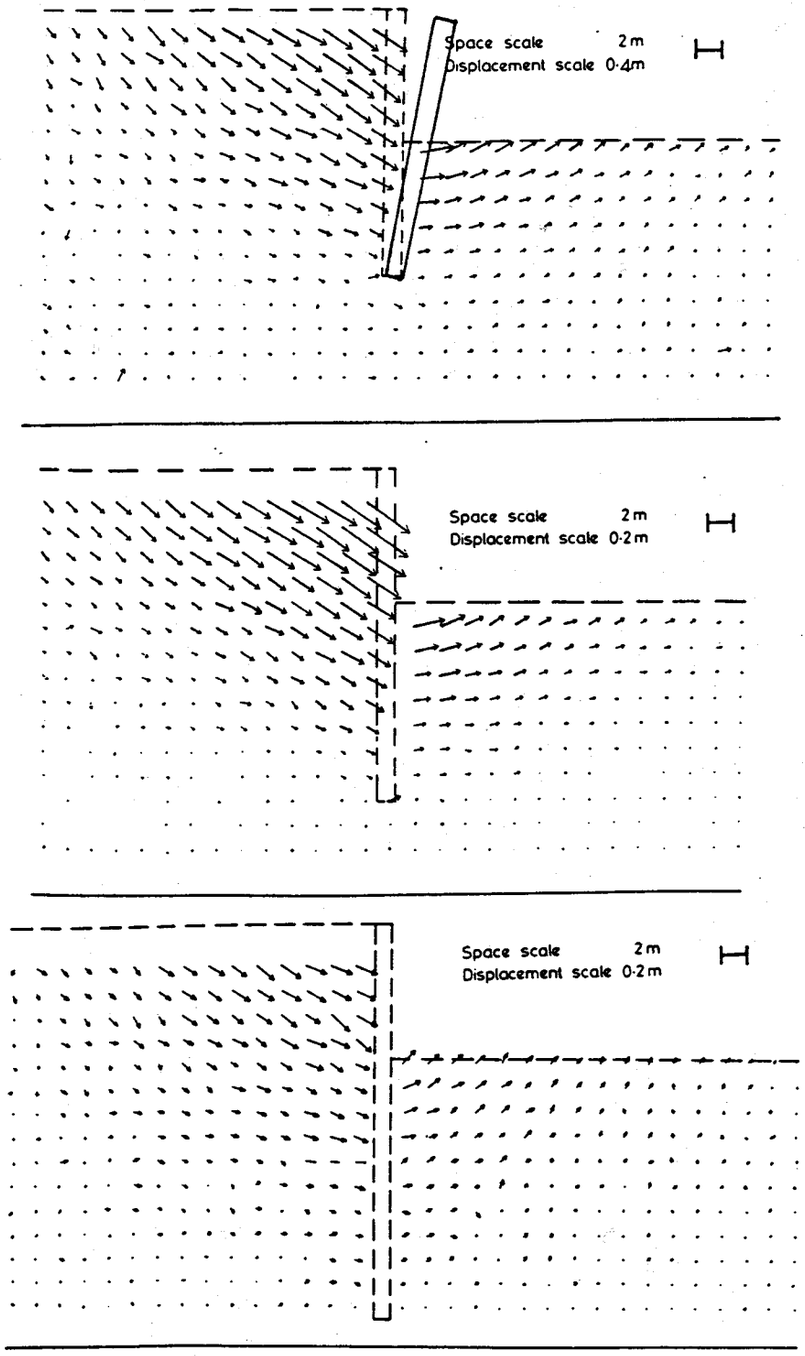

Fig 25 Displacements in over-consolidated clays around model diaphragm walls

discontinuities. A more careful analysis permitting the shear strains on the excavated side to develop at nearly twice the rate of those on the retained side, as indicated by the mechanism, with the mobilisation of consistently different strengths, was shown to be very little different from a simple analysis based on averaged properties and strengths: Bolton and Powrie (1988). Once again, good back-analyses were possible if earth pressures on the two sides of the wall were developed using wall friction.

Although the *magnitude* of soil displacements was of the correct order, the distribution of displacements on the retained side did not feature the step at a separation equal to the wall height. The kinematics in figure 27b replaces the step by a cusp, and creates settlements further from the wall, as was observed. Certainly, the equilibrium analysis of figure 27b would be straightforward. Each circle drawn with a radius r between H and R delivers a calculable torque through its circumference, so the mean mobilised shear stress on the circumference can be found. The shear stress mobilisation with shear strain for each element along the circumference can be determined using compression tests at A, simple shear tests at B and extension tests at C – all on vertically cored samples. Each of A, B and C must shear the same amount according to the mechanism, so the shear strain can be incremented until the average shear stress takes the appropriate value. Finally, the shear strains at the different radii can be numerically integrated to give the rotation of the wall and of any point in the soil. As before, a spread-sheet would be ideally suited to the task.

Long-term equilibration of pore pressures led to reasonable predictions when undrained shear stress t_{mob} was simply replaced by ϕ_{mob}, using the same data of undrained triaxial tests with pore pressure measurement. The same kinematics were employed; only the equilibrium calculations were changed to reflect long-term pore pressures. The justification for ignoring volume change can no longer be made if effective stresses reduce too strongly. Bolton and Stewart (1993) show that significant swelling can occur when groundwater rises, and that the prediction of bending moments for walls (that will be stiffly supported in the long term) can easily be made in a desk calculation by following the bi-linear approximation to the 1D swelling stress path already shown in figure 10.

Conclusions

Finite element analyses are capable of giving good predictions of ground deformations only when the behavioural models used for the soil are capable of fitting the non-homogeneous, anisotropic, non-linear properties observed in stress-strain tests on soil elements. Given the same information, rather direct predictions of earth pressures and ground displacements can be made using the principles of plastic analysis.

While plastic equilibrium equations are universally well understood, the mechanisms used in plastic analysis have been based on sliding wedges and slip circles. These are useless in the analysis of the plastic strain-hardening range of soil behaviour prior to peak strength. The superstition has therefore arisen that plastic analysis can only be carried out at collapse. This is not the case: plastic mechanisms offering familiar equilibrium equations, but based on distributed plastic strains, are relatively easy to generate and have been shown to be quite successful in replicating the main features of ground displacements around retaining walls.

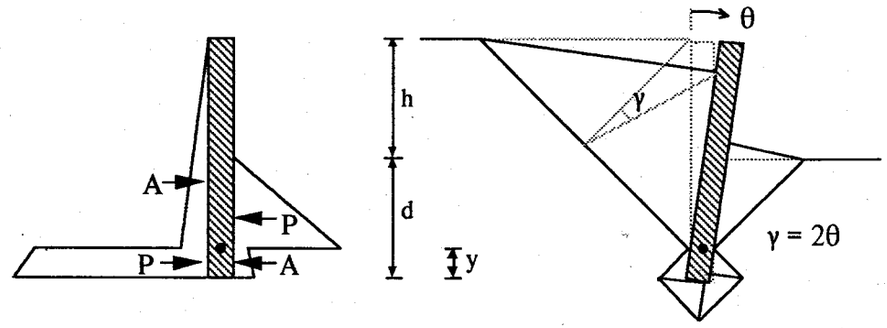

Fig 26 Equilibrium and compatibility in the vicinity of a stiff embedded wall

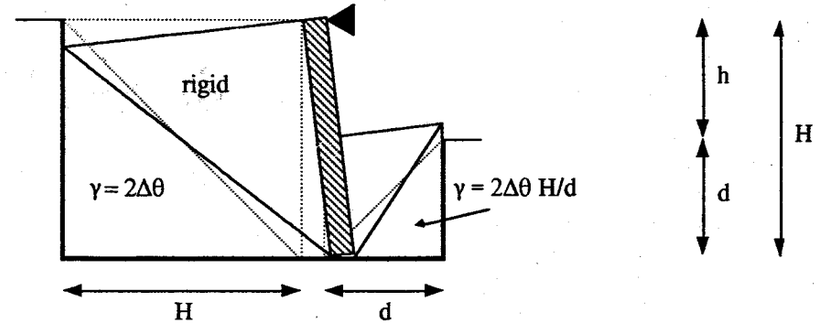

(a) triangular deformation zones bounded by smooth discontinuities

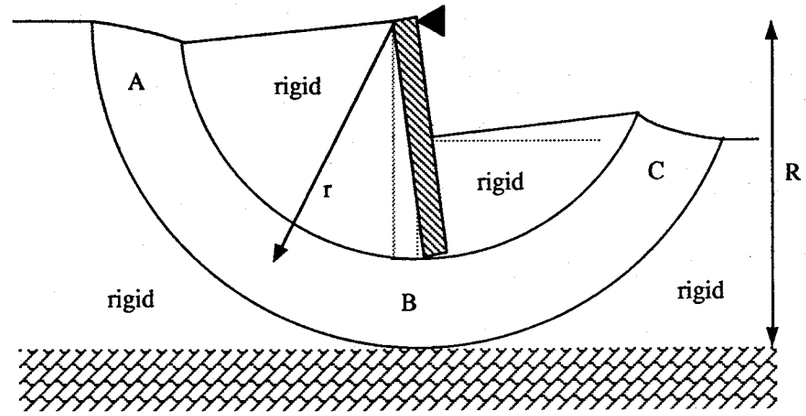

(b) torsional deformation zone

Fig 27 Kinematics for walls propped at the top

It has been shown that compatibility equations are available to link proportional structural displacements with associated soil strains in the surrounding plastic mechanism. A good rule of thumb is that the shear strain is roughly double the relative displacement of structure, defined as the maximum displacement divided by the critical dimension controlling the size of the soil mechanism. A designer can set a target displacement, deduce the permitted soil strain, read off the soil strength mobilised at that strain, and use that strength in conventional plastic equilibrium analyses. If a nominal design calculation is sufficient, a mobilisation factor can be selected to reduce peak strength to a value at which strains should generally be acceptable. The selection of an appropriate factor can take account of the strain to failure, and the degree of non-linearity, by fitting power curves to typical stress-strain data.

It has also been shown to be possible to set out incremental plastic calculations which respect initial earth pressures, soil heterogeneity, and anisotropy. Such calculations certainly need a micro-computer, but a spread-sheet program could accept raw stress-strain data if desired, and can furnish predictions similar to those available with the best non-linear finite element programs. Further centrifuge model studies should enlarge the scope and reliability of all these calculation methods.

Critical uncertainties remain, especially those associated with cracking. Cracking has been presented here as a two-stage phenomenon linked first to the tensile failure of the fluid phase, and to the formation of a frictional shear crack with atmospheric pressure in gas-filled voids, and secondly to the tensile separation of the two sides following the reduction to zero of the normal total stress. Cracking can be understood best in terms of stress-path diagrams in which initial total and effective stresses, both vertical and horizontal, are required. Current practice in fixing crack depths is crude and often erroneous, haphazardly over- or under-conservative. Water-filled cracks can remain open to great depths in clay. Significant failures have occurred due to excavation supports moving sufficiently to permit ground strains which rupture water lines; flooded tension cracks can then lead to the total collapse of the excavation supports. Designers need to be very thoughtful before they deploy supports which would be unable to resist the hydraulic pressure in flooded tension cracks.

The most significant failing in the design of geotechnical works to control deformations remains an unnecessary lack of confidence regarding stress-strain data. Techniques are now available to ensure that data is reliable in the required range of strains, whether tests are conducted in situ by self-boring pressuremeters or in the laboratory in stress-path cells. They should increasingly be used.

References

Bjerrum, L. and Eide, O. (1956) Stability of strutted excavations in clay. Geotechnique, Vol. 6, pp. 32-47.

Bolton, M.D. (1993) What are partial factors for? International Symposium on Limit State Design in Geotechnical Engineering, Copenhagen, Vol. 3, (in press).

Bolton, M.D. and Powrie, W. (1987) The collapse of diaphragm walls retaining clay. Geotechnique, 37, No.3, pp. 335-353.

Bolton, M.D. and Powrie, W. (1988) Behaviour of diaphragm walls in clay prior to collapse. Geotechnique, 38, No.2, pp. 167-189.

Bolton, M.D. and Powrie, W. and Stewart, D.I. (1987) Effects on diaphragm walls of groundwater pressure rising in clays. 9th European Conference on Soil Mechanics and Foundation Engineering, Dublin, Vol. 2, pp. 759-762.

Bolton, M.D., Powrie, W. and Symons, I.F. (1989-90) The design of in-situ walls retaining overconsolidated clay. Part I, Ground Engineering, Vol. 22, No.8, pp. 44-48; Vol. 22, No. 9, pp. 34-40; Part II, Ground Engineering, Vol. 23, No.2, pp. 22-28.

Bolton, M.D. and Stewart, D.I. (1993) The effect on propped diaphragm walls of rising groundwater in stiff clay. Geotechnique, (in press).

Bolton, M.D. and Sun, H.W. (1991a) Designing foundations on clay to limit immediate movements. 4th International Conf. on Ground Movements and Structures, Cardiff.

Bolton, M.D. and Sun, H.W. (1991b) The behaviour of bridge abutments on spread foundations. 10th European Conference on Soil Mechanics and Foundation Engineering, Florence, pp. 319-322.

Bolton, M.D., Sun, H.W. and Britto, A.M. (1993) Finite element analyses of bridge abutments on firm clay. Computers and Geotechnics, (in press).

Burland, J.B., Simpson, B. and St. John, H.D. (1979) Movements around excavations in London clay. 7th European Conference on Soil Mechanics and Foundation Engineering, Brighton, Vol. 1, pp. 13-29.

Bykovtsev, G.I. (1961) On the velocity field in the problem of indentation of a flat punch into a plastic half-space (in Russian). Prikl. Mat. Mekh., Vol. 25, pp. 552-553.

Clough, G.W. and Hansen, L. (1981) Clay anisotropy and braced wall behaviour. Journal of Geotechnical Engineering Division, ASCE, Vol. 107, No. 7, pp. 893-914.

Clough G.W. and O'Rourke T.D. (1990) Construction-induced movements of in situ walls. Design and Performance of Earth Retaining Structures, Geotechnical Special Publication No. 25, ASCE, pp. 439-470.

Eide O., Aas G. and Josang T. (1972) Special application of cast-in-place walls for tunnels in soft clay in Oslo. 5th European Conference on Soil Mechanics and Foundation Engineering, Madrid, Vol. 1, pp. 485-498.

Kimura, T., Takemura, J., Hiro-Oka, A., Suemasa, N., Kouda, N. (1993) Stability of unsupported and supported vertical cuts. 11th Southeast Asian Geotechnical Conference, Singapore, pp. 61-70.

O'Rourke, T.D. (1992) Base stability and ground movement prediction for excavations in soft clay. International Conference on Retaining Structures, U.K. Institution of Civil Engineers, Cambridge, (in press).

Peck, R.B. (1969) Deep excavations and tunnelling in soft ground. 7th International Conference on Soil Mechanics and Foundation Engineering, Mexico City, State-of-the-Art Volume, pp. 225-290.

Prandtl, L. (1920) Über die Härte plastischer Körper. Götinger Nachrichten, mat.phys., p.74.

Schmidt B. (1966) Discussion of "Earth pressures at rest related to stress history" by Brooker and Ireland, Canadian Geotechnical Journal, Vol. 3, No.4.

Szczepinski, W. (1979) Introduction to the mechanics of plastic forming of metals. Sijthoff and Noordhoff International Publishers, The Netherlands, (first published in Polish by PWN, Warsaw, in 1967).

Terzaghi, K. (1943) Theoretical Soil Mechanics. John Wiley and Sons, New York.

Terzaghi, K. and Peck, R.B. (1948) Soil Mechanics in Engineering Practice, John Wiley and Sons, New York.